

ON THE THERMAL INSTABILITY IN A CONTRACTING GAS CLOUD AND FORMATION OF A BOUND CLUSTER

MOTOMICHI TASHIRO AND RYOICHI NISHI

Department of Physics, Kyoto University, Kyoto 606-8502, Japan

tashiro@tap.scphys.kyoto-u.ac.jp, nishi@tap.scphys.kyoto-u.ac.jp

KUNS-1629

ABSTRACT

We perform linear analysis of thermal instability in a contracting large cloud filled with warm H I gas and investigate the effect of metallicity and radiation flux. When the cloud reaches critical density n_f , the cloud fragments into cool, dense condensations because of thermal instability. For a lower metallicity gas cloud, the value of n_f is high. Collision between condensations will produce self-gravitating clumps and stars thereafter. From the result of calculation, we suggest that high star formation efficiency and bound cluster formation are realized in low-metallicity and/or strong-radiation environments.

Subject headings: galaxies: star clusters — globular clusters: general — instabilities

1. INTRODUCTION

The Galactic globular clusters are suggested to be fossil record of the Galaxy formation era (e.g., Fall & Rees 1985). So any knowledge about their formation mechanism will be helpful to understand the protogalactic environment. Young counterparts of globular clusters are absent in the Milky Way, whereas in galaxies such as the LMC, SMC and M33, young globulars exist (e.g., Kumai, Basu, & Fujimoto 1993; Efremov 1995). Such galaxies are in many case ongoing mergers and merger remnants or starburst galaxies, but young globulars also exist in normal spiral, dwarf and irregular galaxies (Schweizer 1999). The conditions that enable globular cluster formation in these galaxies may be also realized at the epoch of the Galactic globular cluster formation. Since globular clusters are gravitationally bound, we attempt to clarify the condition of bound cluster formation.

At the formation epoch of the globular clusters, high star formation efficiency (SFE) must be achieved somehow, since high SFE is required in order to form a bound cluster. The threshold SFE value for bound cluster formation is 0.5 in the case of rapid gas removal (e.g., Hills 1980), which is significantly greater than average SFE (~ 0.01) in the giant molecular clouds (GMCs). Thus, to understand the conditions of bound cluster formation, we should know in what environment the SFE can be high. In regard of this problem, Elmegreen & Efremov (1997) claimed that high-pressure environment is required for bound cluster formation because disruption of the cluster-forming cloud by massive stars is difficult in such an environment. They also argued that bound cluster formation is efficient in a low-metallicity environment, as it is difficult to disrupt the cloud by radiation pressure of massive stars. Here, considering the formation process of dense clouds, we point out that high SFE and efficient bound cluster formation can be achieved in low-metallicity and/or strong-radiation environments because of cloud fragmentation via thermal instability.

Molecular clouds, where stellar clusters form, usually belong to some larger structure such as superclouds (Elmegreen & Elmegreen 1983), the largest cloud complexes in galaxies. Due to the similarity between the masses of superclouds and the critically unstable Jeans mass, large-scale gravitational instability is considered to produce these superclouds (Elmegreen

1987). Warm H I gas occupies large fraction of these superclouds, since roughly half of the H I in the Milky Way disk is in the form of warm gas (Kulkarni & Heiles 1988). When the gas disk becomes gravitationally unstable and fragments into superclouds, this warm gas should be converted into cold H I gas since the gas becomes thermally unstable when the density is somewhat higher. From this cold H I gas, GMCs and, subsequently, stellar clusters are expected to form. Similarly, GMC formation in a supercloud via thermal instability was also considered by Kolesnik (1991). However, his method was based on density structure of static isothermal cloud and our treatment is different.

For modeling the above-mentioned top-down scenario of cluster formation from a supercloud (see also Efremov 1995), we consider a large, warm gas cloud ($T \sim 10^4$ K) contracting because of its self-gravity. As the cloud density increases, it becomes thermally unstable and breaks up into cool, dense condensations. We investigate this process based on linear analysis of thermal instability in the cloud. For the evolution of condensations, we adopt the scenario that these condensations collide each other and self-gravitating clumps are formed in the cloud, and then stellar clusters form. To judge whether the cluster is bound or not, we should know the mean density of the cloud at the point of breakup, since we can relate the mean density of the cloud to its velocity dispersion, which determines SFE and hence whether the cluster is bound or unbound. So we calculate the thermal evolution of a contracting gas cloud and estimate the density when the cloud becomes thermally unstable. The effects of metallicity and radiation flux are also examined.

In the following sections, we present the model of the cloud and the instability analysis method. Based on the results of the calculations, we discuss the conditions necessary for high SFE and bound cluster formation.

2. THERMAL EVOLUTION OF A CONTRACTING GAS CLOUD

We calculate the evolution of density, temperature, and ionization degree of a contracting gas cloud. For simplicity, we consider a spherical and homogeneous gas cloud. As an initial condition, we take the static cloud filled with warm H I gas ($T \sim 10^4$ K) in thermal and ionization equilibrium. The contraction is simplified as a free-fall collapse. Then the thermal

evolution of the cloud is given by the following basic equations:

$$\frac{d}{dt} \ln n = \left\{ 24\pi G \rho \left[1 - \left(\frac{n_i}{n} \right)^{1/3} \right] \right\}^{1/2}, \quad (1)$$

$$\frac{d\varepsilon}{dt} = \frac{P}{\rho} \frac{d\rho}{dt} - \mathcal{L}, \quad (2)$$

$$\frac{dx_e}{dt} = X(T, \rho, x_e). \quad (3)$$

Here ρ and n are the mass and number density of hydrogen of the cloud, respectively, and n_i is the initial value of n . P , T , ε , and x_e are the pressure, temperature, internal energy, and ionization degree of the cloud, respectively. Function \mathcal{L} represents the net cooling rate. As heating sources, we consider interstellar UV radiation, soft X-ray, and cosmic ray. As coolants, we consider hydrogen Ly α cooling, line cooling by O I, C II, Si II, Fe II, dust cooling, and so on. Ionization states of these metal species are fixed according to their ionization potentials. In this work we approximate the cloud as optically thin. Function X represents the net ionization rate of hydrogen atoms. We consider soft X-ray and cosmic ray as ionizing sources. To determine the X-ray heating and ionization rate, the hydrogen column density of the cloud, N_H , must be specified. we take $N_H = 10^{19} \text{ cm}^{-2}$ throughout the cloud evolution, though N_H increases as the cloud contracts. This simplification is not serious, since we performed the same calculation including the change of N_H and got almost the same result. For these thermal processes, we refer to Wolfire et al. (1995) and references there in.

To verify the dependence on metallicity and radiation flux, we introduce parameters Z and X_0 . In our assumptions, the number density of dust grains and the gas phase abundances of O I, C II, etc. change in proportion to Z . The UV radiation flux, X-ray flux and cosmic ray flux change proportional to X_0 . Here $Z = 1$ and $X_0 = 1$ correspond to solar values.

3. FORMATION OF CONDENSATIONS DUE TO THERMAL INSTABILITY

We estimate the mass and the formation timescale of condensations using linear approximation. The growth of density perturbation in the parent cloud is governed by the equation

$$\sigma^3 + \sigma^2 c_s \left(k_T + \frac{k^2}{k_K} \right) + \sigma c_s^2 k^2 + \frac{c_s^3 k^2}{\gamma} \times \left[k_T - k_\rho + \frac{k^2}{k_K} - \frac{\gamma}{c_s^3} (\gamma - 1) \mathcal{L}_0 \right] = 0, \quad (4)$$

where k and σ are the wave number and the growth rate of the perturbation, respectively. This equation is the same as in Field (1965), except in the last term, where it represents nonequilibrium effect. Thus, the net cooling rate $\mathcal{L}_0 = \mathcal{L}(T_0, \rho_0, x_{e0})$ is not necessary zero, where T_0 , ρ_0 , and x_{e0} are the background temperature, density, and ionization degree, respectively. The definitions of k_ρ , k_T , and k_K are the same as in Field (1965):

$$k_\rho = \frac{\mu(\gamma-1)\rho_0\mathcal{L}_\rho}{Rc_sT_0}, \quad k_T = \frac{\mu(\gamma-1)\mathcal{L}_T}{Rc_s}, \quad (5)$$

$$k_K = \frac{Rc_s\rho_0}{\mu(\gamma-1)K_0},$$

where μ , γ , R , and c_s are the mean molecular weight, ratio of specific heats, gas constant, and sound speed, respectively. We

take the value of μ as 1.4 and γ as 5/3. The sound speed is expressed as $c_s = (\gamma P_0/\rho_0)^{1/2}$, where P_0 is the background pressure. The symbols \mathcal{L}_ρ , \mathcal{L}_T , and K_0 are represented as follows:

$$\mathcal{L}_\rho = \left(\frac{\partial \mathcal{L}}{\partial \rho} \right)_T, \quad \mathcal{L}_T = \left(\frac{\partial \mathcal{L}}{\partial T} \right)_\rho, \quad K_0 = K(T_0), \quad (6)$$

where $K(T)$ is thermal conductivity, and we adopt $K(T) = 2.0 \times 10^3 T^{1/2}$, the thermal conductivity for neutral hydrogen.

Among three roots of equation (4), two roots correspond to sound wave modes and one root corresponds to isobaric condensation mode (Field 1965). When this equation has unstable isobaric condensation mode, condensations form because of the growth of unstable perturbations (e.g., Goldsmith 1970). This mode has a maximum growth rate of σ_m at wave number k_m (Fig. 1). Among various density perturbations with different intensities and wave numbers in the cloud, the perturbations with wave number k_m grow fastest. So we estimate the mass of the condensation, M , as

$$M = \frac{4\pi}{3} \rho_0 \left(\frac{\lambda_m}{2} \right)^3, \quad \lambda_m = \frac{2\pi}{k_m}. \quad (7)$$

We also estimate the formation timescale as

$$t_g = \frac{1}{\sigma_m}. \quad (8)$$

Because equation (4) is derived under the assumption that contraction of the cloud is negligible, it must keep in mind that equation (4) is applicable only when the growth timescale of perturbation is shorter than the contraction timescale of the cloud. Also note that our use of equation (4) is justified when λ_m is much smaller than the parent cloud, because equation (4) is for an infinite homogeneous medium. We can neglect this point, since the parent cloud (\gtrsim a few kpc) is much larger than λ_m (\sim a few pc).

4. RESULTS

We perform the calculation in the parameter ranges $Z = 1-10^{-2}$, $X_0 = 10-0.1$. For the purpose of illustration, we show the results of the cases ($Z = 1, X_0 = 1$) and ($Z = 10^{-2}, X_0 = 1$) in Figures 2 and 3. In the figures, evolutionary paths in $n-T$ plane of both the free-fall collapsing gas cloud and the quasi-statically contracting gas cloud keeping thermal equilibrium are presented. Equations (1)-(3) are used for the free-fall collapsing paths and the equations, $\mathcal{L}(T, \rho, x_e) = 0$ and $X(T, \rho, x_e) = 0$, are used for thermal equilibrium paths. The condensation mass M and t_g/t_{dyn} , the ratio of formation timescale of condensation to dynamical timescale of the parent cloud, are also shown in the same figures. Here the dynamical timescale of the parent cloud, t_{dyn} , is defined as $\rho / (d\rho/dt)$, where ρ is the density of the parent cloud. The contours of M and t_g/t_{dyn} in Figures 2 and 3 are calculated using equation (4), with the assumption of ionization equilibrium (i.e., only n and T are used for calculation, and x_e is a function of n and T). From the figures we can see the tendency that the smaller metallicity, the more the evolutionary path of the free-fall collapsing cloud deviates from the path of the quasi-statically contracting cloud. For the case $Z = 1$, the two evolutionary paths deviate in temperature $\sim 1000\text{K}$ at density $\sim 1 \text{ cm}^{-3}$. In contrast, for the case $Z = 10^{-2}$, the two paths deviate $\sim 8000\text{K}$ at density $\sim 100 \text{ cm}^{-3}$. For the paths of the free-fall collapsing gas cloud, dependence on metallicity is stronger than equilibrium paths. Such behavior is explained by the fact that a nonequilibrium state is realized for free-fall cases because the cooling timescale can be long relative to dynamical time and that degree of nonequilibrium is stronger for lower metallicity since cooling time is in inverse proportion to Z .

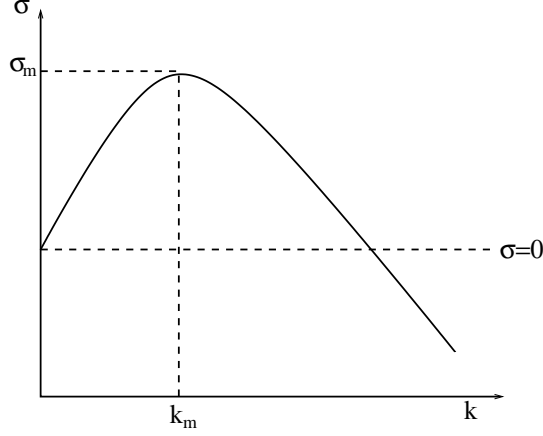


FIG. 1.— Dispersion relation of thermal instability (schematic example). Among three modes, only condensation mode is presented. Since the region $\sigma > 0$ exists, this mode is unstable and condensations are formed from density perturbations with positive σ . Note that there exists a maximum growth rate σ_m at wave number k_m .

As the cloud density exceeds some critical value, the gas cloud becomes thermally unstable. At this point, the growth timescale of perturbation, t_g , is longer than the dynamical timescale of the cloud, t_{dyn} . So the perturbation cannot grow to the condensation, because the parent cloud evolves faster than the perturbation. As the cloud evolves, t_g becomes smaller than t_{dyn} . Thus, condensation will form at the moment $t_g = t_{\text{dyn}}$. For the case $Z = 1$, condensations form at the density $\sim 1 \text{ cm}^{-3}$ (Fig. 2a), whereas for the case $Z = 10^{-2}$, condensations form at the density $\sim 300 \text{ cm}^{-3}$ (Fig. 3a). Condensation mass is a few $10M_{\odot}$ at the density $\sim 1 \text{ cm}^{-3}$ for $Z = 1$ (Fig. 2b) and a few M_{\odot} at the density $\sim 300 \text{ cm}^{-3}$ for $Z = 10^{-2}$ (Fig 3b).

For the case when Z and X_0 are simultaneously changed, the results are shown in Figure 4. The calculational procedure for Figure 4 differs from Figures 2 and 3, in a point that t_g and M are calculated using equations (1)-(8) to draw Figure 4, whereas the assumption of ionization equilibrium is adopted to draw the contours of Figures 2 and 3. In Figure 4a, the cloud density n_f at the time of condensation formation is shown. For $X_0 = 1$, the density n_f increases from $\sim 1 \text{ cm}^{-3}$ at $Z = 1$ to $\sim 300 \text{ cm}^{-3}$ at $Z = 10^{-2}$. For $Z = 1$, n_f increases from $\sim 0.1 \text{ cm}^{-3}$ at $X_0 = 0.1$ to $\sim 10 \text{ cm}^{-3}$ at $X_0 = 10$. In Figure 4b, the condensation mass is shown. For $X_0 = 1$, the mass M decreases from $\sim 30M_{\odot}$ at $Z = 1$ to $\sim 1M_{\odot}$ at $Z = 10^{-2}$. For $Z = 1$, M decreases from $\sim 300M_{\odot}$ at $X_0 = 0.1$ to $\sim 1M_{\odot}$ at $X_0 = 10$. Thus, from Figure 4, we can see that for the smaller metallicity, the cloud density n_f is the larger, and the condensation mass M is the smaller. We can also see that for the stronger radiation, the density n_f is the larger and the mass M is the smaller.

Previously, Elmegreen & Parravano (1994) calculated the critical pressure for coexistence of cool and warm gas, changing radiation flux and metallicity. This critical pressure roughly corresponds to n_f in this work. Contrary to our results, metallicity dependence of the critical pressure is small in their calculation. They assumed static cloud for the background, whereas we assume free-falling cloud. Then, as noted above, for the smaller metallicity, the evolutionary path of free-fall contracting cloud deviates more from the path of the quasi-statically contracting cloud, because of the reduced cooling rate. On the other hand, for the static cloud, thermal equilibrium is achieved so that metallicity dependence is weak. This is the reason of the difference between our work and their work.

We estimate the density of condensation as follows. After

the criterion $t_g = t_{\text{dyn}}$ is achieved, the overdensity region (size $\sim \lambda_m$) in the parent cloud grows in pressure equilibrium with surrounding gas, since crossing time is short compared with cooling time for the fastest growing perturbation. Then the overdensity evolves along an isobaric path starting from the point $t_g = t_{\text{dyn}}$ (this path is not drawn in Figs.2 and 3). The runaway growth of the overdensity continues until it reaches thermochemical equilibrium, where it is thermally stable (e.g., Parravano 1987). We search the intersection of the isobaric path (the path with $nT = \text{constant}$, starting from the point $t_g = t_{\text{dyn}}$) with the equilibrium path (Figs.2 and 3, *dashed line*) and identify it as “condensation”. From the intersection, we can know the density of condensation, n_c , and the temperature of the condensation, T_c . We perform the calculation and find that n_c is roughly 100 times larger than n_f in most parameter ranges. In the above-described procedure, we assume that the intersection is thermally stable and self-gravity of the overdensity can be neglected. We confirm that all intersections in this calculation are thermally stable, so that the first assumption is justified. The second assumption is also justified by the later discussion. Using the values of n_c and T_c , the Jeans mass can be derived, and it is much larger than the condensation mass for most parameter values. Thus, self-gravity of the condensation is negligible and the density inside the condensation is expected to be almost uniform. After formation, condensations accrete surrounding gas and can potentially grow to be self-gravitating. To estimate the mass growth rate of condensation, we should calculate the rate of mass flow across the boundary between the condensation and surrounding gas. According to previous works (e.g., Penston & Brown 1970; Parravano 1987), the growth timescale of the condensation mass is much larger than the free-fall timescale of the parent cloud. So we can neglect the mass growth of condensation through accretion.

5. APPLICATION TO BOUND CLUSTER FORMATION

After formation of condensations, the parent cloud continues free-fall contraction until collisions between condensations begin. Then the formation of massive self-gravitating clumps through collisional buildup of small condensations is expected. Star formation inside such massive clumps will follow. However, evaluation of such evolution is difficult task. The onset of collisions depends on velocity distribution and space density of condensations, which we cannot know precisely. Subsequent

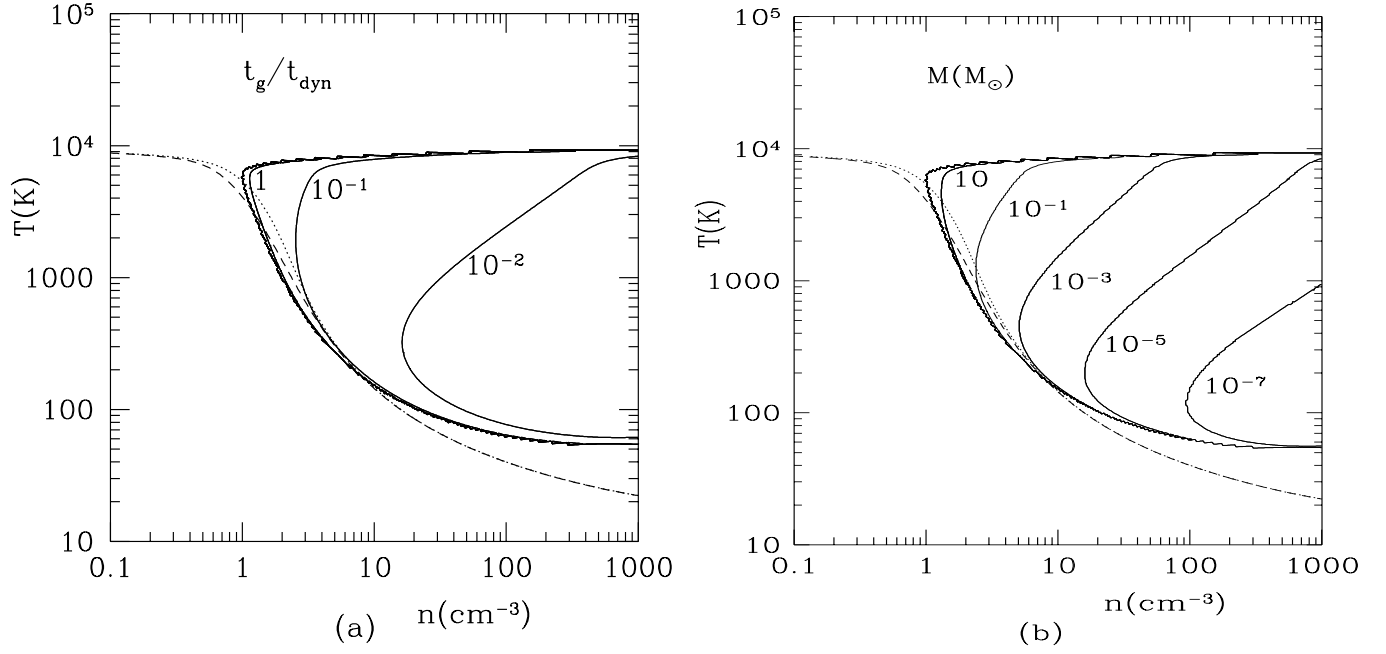


FIG. 2.— (a) Ratio of formation timescale of condensation, t_g , to dynamical timescale of the cloud, t_{dyn} , is shown in $n-T$ as solid contours. The dynamical time t_{dyn} is defined as $\rho_0 / (d\rho_0/dt)$, where ρ_0 is the density of the cloud. Numbers near the contours represent the values of t_g/t_{dyn} . Metallicity and radiation parameters are $Z = 1$ and $X_0 = 1$, respectively. The thermally unstable region is inside the most outer contour. We calculate the contours under the assumption of ionization equilibrium. Thermal evolution of the free-falling cloud is presented in the plane as a dotted line. For reference, we also show thermal evolution of the quasi-statically contracting cloud keeping thermal equilibrium as a dashed line. (b) Condensation mass $M(M_\odot)$ is shown in $n-T$ plane as solid contours for the same parameters. Numbers near the contours represent the values of $M(M_\odot)$. Meanings of dashed and dotted lines are the same as in Fig. 2a.

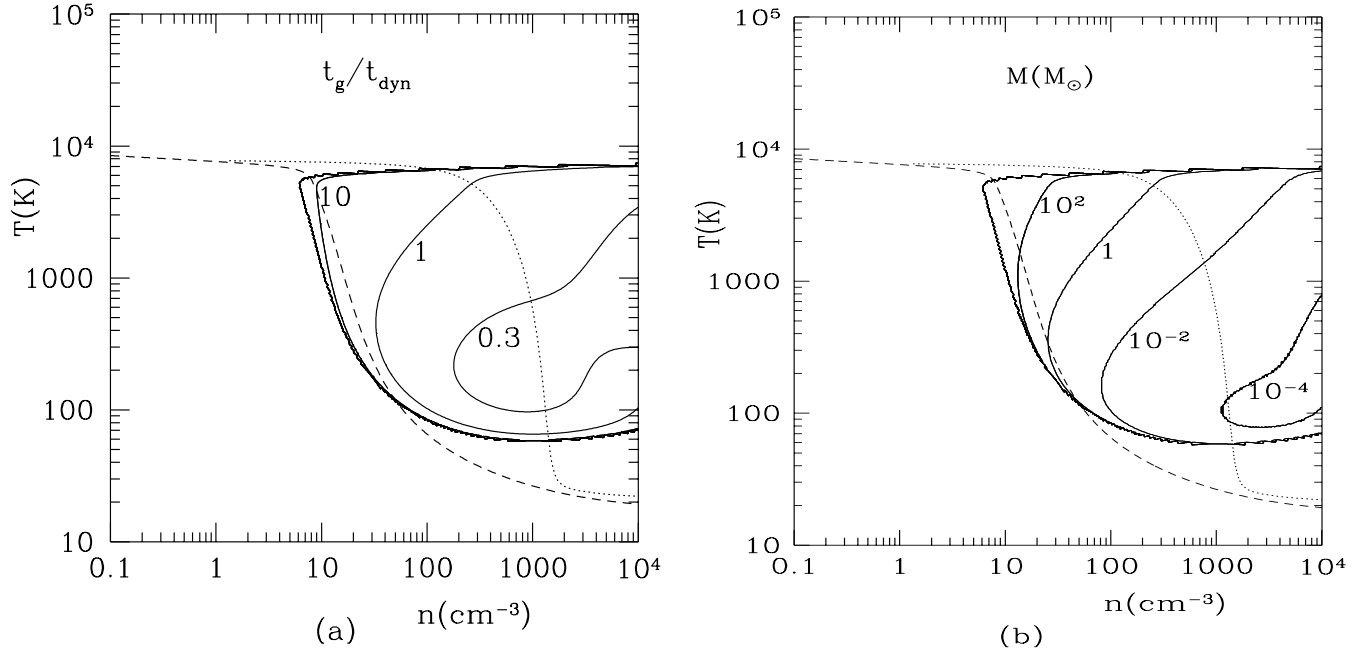


FIG. 3.— Same as Fig. 2, but the metallicity parameter is $Z = 10^{-2}$. The evolutionary path of free-fall collapse case deviates far from the path of quasi-statically contracting case.

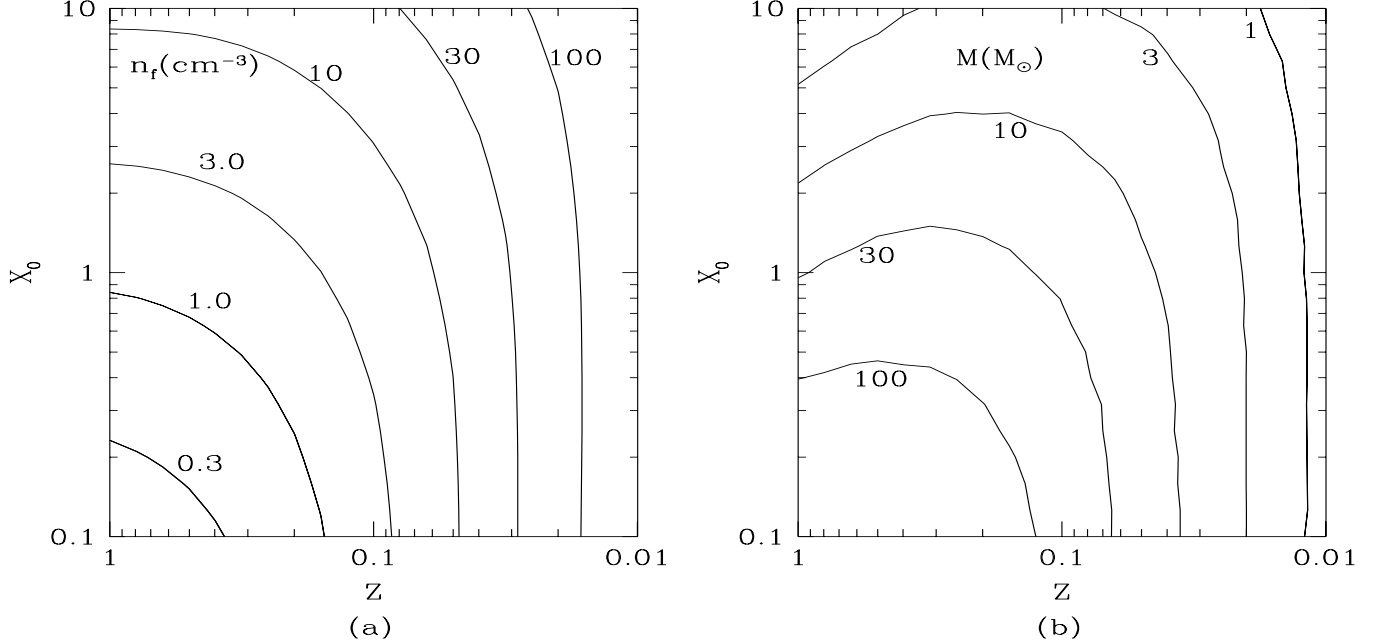


FIG. 4.— (a) Cloud density $n_f(\text{cm}^{-3})$ at the time of condensation formation is presented in X_0 - Z plane as contours. Numbers near the contours represent $n_f(\text{cm}^{-3})$. We assume that condensations form at the moment $t_g = t_{\text{dyn}}$, where t_g is the formation timescale of condensation and t_{dyn} is the contraction timescale of the cloud. (b) Condensation mass $M(M_\odot)$ at the time of its formation is presented in X_0 - Z plane as contours. Numbers near the contours represent $M(M_\odot)$.

evolution of condensations also depends on velocity and mass distribution of condensations through the collisional process. This collisional process is not so simple (e.g., Hausman 1981) and makes the calculation of evolution complicated. In regard of these difficulties, we adopt a simplified picture of the evolution of condensations. We neglect the random velocity of condensations and assume homologous contraction of the parent cloud composed of condensations. Then the collisions begin when the mean parent cloud density increases to the density of condensation, n_c , because the parent cloud is almost filled with condensations in such situation. As a result of collisions (we assume that the output of collision is mostly adhesion), massive self-gravitating clumps will form. At this point, the density of massive clumps is larger than the mean parent cloud density n_c , because of self-gravity. So the parent cloud contract further. We assume collisionless collapse of the system composed of self-gravitating clumps, for simplicity. Then the virialization of the system and the beginning of star formation in the clumps is expected.

It is reasonable to consider that the cluster-forming region is only a part of the parent cloud, not the entire cloud. We define the mass of the region as M_{cl} and take the reference value as $10^5 M_\odot$ according to typical mass of globular clusters. Then virial velocity of the region is

$$c \sim 2 \times \left(\frac{M_{\text{cl}}}{10^5 M_\odot} \right)^{1/3} \left(\frac{n_{\text{cl}}}{1 \text{cm}^{-3}} \right)^{1/6} \text{ km s}^{-1}, \quad (9)$$

where n_{cl} is the mean hydrogen number density of the cluster-forming region. Because (1) we assume collisionless collapse of the parent cloud composed of self-gravitating clumps, where the mean cloud density at the onset of collapse is the same as condensation density n_c , and (2) condensation density n_c is typically 100 times higher than the parent cloud density at the time of condensation formation, n_f (see the last paragraph in § 4), n_{cl} and n_f are related as

$$n_{\text{cl}} \sim 800 n_f, \quad (10)$$

where the relations, $n_{\text{cl}} \sim 8 n_c$ from the point (1) and $n_c \sim 100 n_f$ from the point (2), are used.

Whether the cluster is bound or not depends on SFE, the ratio of stellar mass to the mass of cluster-forming region. And SFE is determined by the interaction between stellar activity and the cluster-forming region. For example, stellar wind, radiation pressure, ionization pressure of the H II region or supernova explosion may blow off remaining gas and lead to lower SFE. In this paper we consider two cases, gas removal by the expanding H II region and supernova explosion.

First we discuss gas removal by expanding H II region. The pressure of H II region corresponds to velocity dispersion $c_{\text{HII}} \sim 10 \text{ km s}^{-1}$. If virial velocity of the region, c , is smaller than c_{HII} , the H II region pushes out the surrounding gas and blows it off, and then the cluster will be unbound. In opposite case, the H II region cannot blow off the surrounding gas and high SFE can be achieved; then the cluster will be bound. So the criterion of bound cluster formation is considered as $c > c_{\text{HII}}$. This corresponds to the condition

$$n_f > 10 \times \left(\frac{C}{800} \right)^{-1} \left(\frac{c_{\text{HII}}}{10 \text{ km s}^{-1}} \right)^6 \left(\frac{M_{\text{cl}}}{10^5 M_\odot} \right)^{-2} \text{ cm}^{-3}, \quad (11)$$

where C represents density enhancement, i.e., the ratio of n_{cl} to n_f . Note that derivation of equation (11) relies on some rough assumptions and depends on uncertain factors such as C , c_{HII} , and M_{cl} . Moreover, dependence on c_{HII} is very strong. So we should regard equation (11) as qualitative criterion.

Next we discuss gas removal by supernova (SN) explosion. The proto-globular cluster cloud is disrupted by several to tens of concurrent SN explosions (Dopita & Smith 1986; Morgan & Lake 1989). A high star formation rate at the formation epoch of globular cluster will cause such multiple SN explosions so that relic gas will be blown off. When the star formation time scale t_{SF} is shorter than the lifetime of massive star, τ , a large

fraction of gas in the cluster-forming region can be converted into stars before SN explosions; then high SFE is achieved and a bound cluster can be formed. In contrast, when t_{SF} is longer than τ , SN explosions will remove surrounding gas and stop later star formation. In this case, low SFE and unbound cluster formation is expected (e.g., Yoshii and Arimoto 1987). The star formation timescale t_{SF} is expected as

$$t_{\text{SF}} = A t_{\text{ff}}, \quad (12)$$

where A represents a proportional constant of order 1 and $t_{\text{ff}} = (3\pi/32G\rho)^{1/2}$ is free-fall timescale of the cluster-forming region. We adopt the lifetime of massive star, τ , as

$$\tau \sim 5 \times 10^6 \text{ yr}. \quad (13)$$

The star formation timescale t_{SF} , evaluated at density n_{cl} , is

$$t_{\text{SF}} = A t_{\text{ff}} \sim 1.3 \times 10^7 A \left(\frac{n_{\text{cl}}}{10^3 \text{ cm}^{-3}} \right)^{-1/2} \text{ yr}. \quad (14)$$

Thus, the condition for high SFE ($\tau > t_{\text{SF}}$) in term of n_f is

$$n_f > 10 \times \left(\frac{\tau}{5 \times 10^6 \text{ yr}} \right)^{-2} \left(\frac{A}{1} \right)^2 \left(\frac{C}{800} \right)^{-1} \text{ cm}^{-3}. \quad (15)$$

This criterion is qualitative, since it depends some uncertain factors, the same as equation (11).

For both case, $n_f > 10 \text{ cm}^{-3}$ is required for high SFE and bound cluster formation. From Figure 4a we can see that the density n_f increases as metallicity decreases and also as radiation increases. The condition $n_f > 10 \text{ cm}^{-3}$ corresponds to the parameter range $Z \lesssim 0.05$ for $X_0 = 1$ and $X_0 \gtrsim 8$ for $Z = 1$. This means high SFE and efficient bound cluster formation are realized in a low-metallicity and/or strong-radiation environment in our model. From Figure 4a, we can also see that when $Z \sim 1$, n_f is more sensitive to X_0 than Z and when $Z \lesssim 0.1$, n_f is more sensitive to Z than X_0 . Thus SFE mainly depends on X_0 around $Z \sim 1$ and on Z below $Z \sim 0.1$.

The qualitative behavior of the above result will be independent of the details about evolution of condensations and feedback from star formation, since the essential ingredients are only two points, (1) low-metallicity and/or strong-radiation fields lead to high breakup density of the parent cloud, and (2) high-density environments result in high SFE. However, our conclusion may be changed if we consider nonspherical evolution of the cloud. The dynamical timescale of an initially nonspherical cloud or a cloud with rotation is similar to that of a spherical cloud at first, e.g., $t_{\text{dyn}} \propto n^{-1/2}$, where n is the density of the cloud. But later disklike collapse will follow and the dynamical timescale becomes $t_{\text{dyn}} \propto n^{-1}$ (Susa, Uehara, & Nishi 1996). Then the ratio of the cooling time $t_{\text{cool}} \propto n^{-1} Z^{-1}$ to the dynamical time is

$$\frac{t_{\text{cool}}}{t_{\text{dyn}}} \propto n^{-1/2} Z^{-1}, \quad (16)$$

for initial spherical-like phase and

$$\frac{t_{\text{cool}}}{t_{\text{dyn}}} \propto Z^{-1}, \quad (17)$$

for later disklike phase. When the cloud becomes thermally unstable, we can estimate whether or not condensations form, using the value of $t_{\text{cool}}/t_{\text{dyn}}$. If this ratio is less than unity, condensation will form, and vice versa. In case the cloud becomes unstable when it is still in a spherical-like phase, condensations will form regardless of the metallicity Z , as we calculated in

this work. This can be explained since the density n , when the cloud becomes unstable, increases as Z decreases (see Figs. 2 and 3), so that $t_{\text{cool}}/t_{\text{dyn}}$ does not change so much. But, in case the cloud becomes unstable when it is in a disklike phase, condensations may not form for the low-metallicity case since $t_{\text{cool}}/t_{\text{dyn}}$ increases as Z decreases. In this case our discussion in this section is not applicable. To summarize, in the presence of rotation or deviation from spherical symmetry, if the cloud becomes thermally unstable in the early phase of collapse, condensations will form and our conclusion in this section is adequate. In contrast, if the cloud becomes thermally unstable in the late phase of collapse, condensations may not form throughout the collapse and another discussion may be required.

Finally, we present some applications. A low-metallicity environment is realized in dwarf galaxies and in the early stage of our Galaxy, for example. And strong-radiation fields are realized in starburst galaxies and probably in the early stage of our Galaxy, where young bulge stars are expected to provide strong radiation. Thus, according to the result, young globular clusters in dwarf galaxies and starburst galaxies may be produced through the mechanism we show in this work. Also, the disk population of globular clusters in our Galaxy (Zinn 1985) may be produced through the same mechanism.

6. SUMMARY

In this paper we perform linear analysis of thermal instability in a collapsing warm gas cloud and study the effect of metallicity and radiation flux. For the calculation, we adopt a one-zone approximation and the cloud contraction is simplified as free-fall collapse. When the cloud density reaches critical value n_f , the cloud fragments into cool dense condensations via thermal instability. From our calculation, the critical density n_f increases as metallicity decreases, and also as radiation increases. Condensations collide with each other and self-gravitating clumps will be produced when the mean cloud density becomes sufficiently high; then stars will form. Expansion of the H II region around the massive star and supernova explosions will blow off surrounding gas and stop star formation process. When the mean density at the time of star formation is high, high virial velocity prevents expansion of the H II region. Also, in such high-density environments, the star formation timescale is shorter than the lifetime of a massive star. Then the gas in cluster-forming region will be converted into stars efficiently, before the gas is dispersed by expanding H II region or supernova explosions. In our calculation, such high density is realized in the contracting low-metallicity gas. And if the formation of a contracting gas cloud is possible, a strong-radiation environment is another candidate. Thus, it is suggested that high star formation efficiency and bound cluster formation are likely achieved in low-metallicity and/or strong-radiation environments. Such environments exist in dwarf galaxies, the early stage of our Galaxy and starburst galaxies. According to the result, globular clusters in these galaxies may be produced through the mechanism we show in this paper.

We would like to thank H. Sato for valuable comments and H. Kamaya for useful discussion. This work is supported in part by the Japanese Grant-in-Aid for Scientific Research on Priority Areas (No. 10147105) of the Ministry of Education, Science, Sports and Culture of Japan.

REFERENCES

- Dopita, M., & Smith, G. H. 1986, *ApJ*, 304, 283
Efremov, Y. N. 1995, *AJ*, 110, 2757
Elmegreen, B. G. 1987, *ApJ*, 312, 626
Elmegreen, B. G., & Elmegreen, D. M. 1983, *MNRAS*, 203, 31
Elmegreen, B. G., & Efremov, Y. N. 1997, *ApJ*, 480, 235
Elmegreen, B. G., & Parravano, A. 1994, *ApJ*, 435, L121
Fall, S. M., & Rees, M. J. 1985, *ApJ*, 298, 18
Field, G. B. 1965, *ApJ*, 142, 531
Goldsmith, D. W. 1970, *ApJ*, 161, 41
Hills, J. M. 1980, *ApJ*, 225, 986
Kolesnik, I. G. 1991, *A&A*, 243, 239
Kulkarni, S., & Heiles, C. 1988, in *Galactic and Extragalactic Radio Astronomy Second Edition*, ed. G. L. Vershuur, & K. I. Kellermann (New York: Springer-Verlag), 95
Kumai, Y., Basu, B., & Fujimoto, M. 1993, *ApJ*, 404, 144
Morgan, S., & Lake, G. 1989, *ApJ*, 339, 171
Parravano, A. 1987, *A&A*, 172, 280
Penston, M. V., & Brown, F. E. 1970, *MNRAS*, 150, 373
Schweizer, F. 1999, to appear in proceedings of a workshop "Spectrophotometric Dating of Stars and Galaxies" (astro-ph/9906488)
Wolfire, M. G., Hollenbach, D., McKee, C. F., Tielens, A. G. G. M., & Bakes, E. L. O. 1995, *ApJ*, 443, 152
Yoshii, Y., & Arimoto, N. 1987, *A&A*, 188, 13
Zinn, R. 1985, *ApJ*, 293, 424